



Optimisation of part orientation and design of support structures in laser powder bed fusion

Mattia Mele¹ · Giampaolo Campana¹ · André Bergmann²

Received: 10 November 2020 / Accepted: 10 February 2022 / Published online: 2 March 2022
© The Author(s), under exclusive licence to Springer-Verlag France SAS, part of Springer Nature 2022

Abstract

Part orientation and support structures are crucial to the quality of metal parts by laser powder bed fusion. Computer-aided solutions for part orientation can be used to support users during the process preparation. In this study, an original computer-aided approach to prepare parts for laser powder bed fusion was formulated and implemented. The proposed method consists of multi-objective optimisation of part orientation and a novel strategy for the simultaneous design of support structures. The automated part orientation optimisation considers both global and local objectives defined by the user. For this purpose, penalty functions measuring the building time, support volume, part distortion, surface roughness and supports contact points are adopted. Unlike in existing methods, the user has the opportunity to define the importance of these aspects in different regions of the part. Such functions are then optimised through a genetic algorithm. The proposed approach was applied to a real product imposing three different sets of objectives. The tested case studies were solved in less than 10 min, providing solutions that satisfied the imposed aims and constraints. Specifically, the results demonstrated that the orientation optimisation can reduce the building time by 68.1% or the material consumption by 66.8%, depending on user requirements. It was also shown how the proposed method can be used to minimise the surface and dimensional error of manufactured parts. The proposed approach allows to manually define the specific design requirements and translate them in terms of manufacturing decisions. This contributes to establishing a fruitful interaction between the user and the developed software during the process design.

Keywords Additive manufacturing · Support structures · Part orientation · Laser powder bed fusion

1 Introduction

Additive manufacturing (AM) comprises several innovative technologies, which are rapidly transforming the industrial scenario [1–3]. Among these processes, metal AM plays a crucial role due to the enormous importance of metallic parts in most mechanical applications [4].

Laser powder-bed fusion (LPBF) is far the most popular technology for the AM of metallic parts starting from

powders [5,6]. This process allows the manufacturing of a wide range of materials to obtain parts characterised by high density and mechanical resistance [7,8]. In recent years, industrial apparatuses for LPBF have tremendously improved [9,10]. Also, numerous studies have focused on the determination of optimal process parameters for the achievement of high-performance products [11,12]. In fact, it has been demonstrated that the laser parameters and scanning strategies play a fundamental role to determine the microstructure and properties of the manufactured parts [13–16].

The arrangement of parts within the building chamber is also fundamental to ensure manufacturability and part quality [17,18]. In greater detail, the orientation of parts and the design of support structures are crucial to the surface quality of parts, building time and process cost [19–21].

As a consequence, numerous studies have focused on automated part orientation [22] and the design of support structures [23]. Most of the approaches in the body of the literature separately manage part orientation and support

✉ Mattia Mele
mattia.mele@unibo.it

Giampaolo Campana
giampaolo.campana@unibo.it

André Bergmann
andre.bergmann@ipk.fraunhofer.de

¹ Department of Industrial Engineering, University of Bologna, Viale del Risorgimento 2, 40136 Bologna, Italy

² Fraunhofer Institute for Production Systems and Design Technology, Pascalstraße 8 - 9, 10587 Berlin, Germany

design, although they are deeply interdependent. Moreover, the objective functions are frequently defined on the entire part geometry, thus failing to address the local product requirements. These aspects are discussed in greater detail in Sect. 2, which provides an overview of the body of literature.

This study introduces a new interactive method for the simultaneous optimisation of part orientation and support design. The method adopts the building time, material volume and surface quality as objectives of the optimisation. Also, the user is given the opportunity to define local constraints and aims, in order to adjust the objective function based on the specific product requirements. Genetic Algorithms (GA) are finally used to determine the optimal solution based on the defined aims.

The proposed method is detailed in Section 3 and applied to a case study in Sect. 4 in order to prove its effectiveness.

2 State of the art

2.1 Build time estimation

The building time duration is one of the main cost drivers in AM [24,25]. For this reason, several methods for its estimation have been proposed in the body of literature.

All the studies in this field have highlighted that the number of layers N_L , and therefore the height along Z direction h_{max} , is the most influential factor on the process duration [26,27]. In laser-based processes, this is also affected by the length of the scanned path. To consider this aspect, several models include the area of each layer in the computation of the build time [27–29].

Rickenbacher et al. [30] proposed an interpolation including, besides h_{max} , the part volume and the surface of parts and supports. Di Angelo et al. [31] elaborated such parameters through a neural network in order to reach a more accurate estimation of the building time.

In the present study, build time is evaluated only for the comparison of alternative solutions and then normalised to compose the final fitness function. Therefore, a simplified estimation based on the maximum height h_{max} is implemented. Details of the calculation are presented in Sect. 3.2.2.

2.2 Surface roughness

One of the main limitations to the industrial applications of parts manufactured via LPBF is the surface quality [32,33]. This is known to be mainly influenced by the surface orientation to the building direction [21,34]. The body of research demonstrates that the optimal surface roughness on upward surfaces is achieved for 0° angles, i.e. regions with normal vector oriented along Z-axis. In the case of non-null

inclinations, the roughness decreases while the angle increases in the range $]0^\circ; 90^\circ]$ [35]. The same considerations can be applied to downward surfaces, where the roughness decreases moving from flat to vertical surfaces. The downward surfaces quality is worse than the one of upward ones as the molten material tends to drop down under the effect of gravity [36,37].

The actual value of surface roughness is also deeply influenced by scanning strategy and laser parameters, especially in downward surfaces [38]. Recently, Rott et al. [39] demonstrated the interdependency of surface orientation and laser incidence using a nickel–chromium-based superalloy.

An exact prediction on the surface roughness must thus consider the set of process parameters and the material features. Such an accurate result is out of the scope of the present work, where a comparative analysis of different solutions is required. In this study, a normalised model reflecting the consideration presented above is developed for comparison. Its equation is introduced in Sect. 3.2.5.

2.3 Automated part orientation and support design

Several methods for the automated determination of the optimal build orientation were proposed in the body of the research since the end of the 20th century. The early methods scanned a finite number of possible orientations and ranked them based on the objective function [24,40,41]. A similar approach was recently revised by Leutenecker-Twelsiek et al. [42]. Such methods select the best orientation within an initial batch of orientations, which may not correspond to the optimal solution. Masood et al. proposed a technique to generate candidate solutions through the incremental variation of orientation angles [43]. More recently, several iterative methods for part orienting have been presented in order to increase the probability to reach the absolute optimum [44,45].

Since the build orientation is chosen considering a number of different requirements, it can be represented as a Multi-Objective Optimisation (MOO) problem the solution of which is a Pareto front of non-dominated solutions [46,47]. Nonetheless, only one orientation can be used for part production. Therefore, the downside with this approach is that the solution must be selected among non-dominated ones by the user [48] or through another selection algorithm [49–52]. To surpass this limitation, the objectives of the optimisation are frequently combined in a single weighted function in order to assign relative importance to each objective and output a single optimal solution [53–55]. This approach gives the user the possibility to adapt the objective function himself to the requirements of the manufactured product and according to his level of knowledge. Since the quality of the proposed solution depends on the manually defined weights given to requirements, the method proposed in this paper adopts an interactive approach. The user can refine these values

iteratively until a satisfactory solution is met. This iterative process also contributes to an increase in the user's know-how about the process. This interactive approach allows for a combination of software capabilities and human expertise [22,56].

The single function optimisation problem has been solved by several authors through GA [57,58]. This approach allows the inclusion of different objective functions and does not require assumptions on the initial orientation of parts [59–61].

The objectives of the optimisation algorithms proposed for LPBF usually comprise the reduction of support volumes and building time, which are the main drivers of process cost [62–64]. These methods assume an orientation-independent design of support structures.

By contrast, this study includes a novel approach to the design of the support structures based on the part orientation. The main advantage of this approach is to ensure efficient use of the support material while rotating the part.

The orientation of parts has also been proven to be crucial to the part distortions induced by the process [65,66]. In fact, the internal stresses inducing the part deformation mainly derive from the temperature distribution, which in turn depends on part orientation and laser strategies [67]. The part orientation also affects the mechanical properties of manufactured products both in terms of static [68–71] and fatigue resistance [72,73]. The optimisation of these properties should take into account the stress distribution inside the part during usage, for example by means of Finite Element Analysis (FEA). This kind of analysis is not included in the present work and is left as an area for further research.

In the optimisation methods mentioned above, the relevance of each objective is defined on the entire model. This may determine a limitation to practical applications, where the requirements of each region depend on the function of the manufactured part. In order to surpass this limit, Ga et al. [54] proposed a method where the user can select the part which must meet the best surface quality. Other authors predefined a set of features (e.g. holes or joints) in which the maximum surface quality must be achieved [74,75]. Recently, automated methods to cluster triangular elements of orientation have been proposed in the literature [76,77]. The full automation of these methods reduces the efforts of the user but limits the opportunity to customise the objectives of the optimisation. To surpass this limitation, this study allows the user to manually assign the importance of each requirement in different part regions. This non-uniform definition of features is presented in Sect. 3.2.5. The main advantage of the proposed approach is to establish an interaction between the user and software to achieve full customisation of the optimisation function. This allows the user to bring specific know-how within the optimisation. For example, it is possible to specify which regions should be preserved by

support structures under the light of the available equipment for support removal. This is not possible in existing fully-automated methods, which consider a single predetermined post-processing strategy [78,79].

2.4 Design of support structures

Thermal stresses occurring during LPBF tend to warp the solidified material out of the plane of the layer. If the distortion of the layer is not tackled, the warped part might become an obstacle for the powder recoater, causing the failure of the entire process. For this reason, it is necessary to build support structures anchoring overhang geometries to the building platform. These offer a mechanical resistance to thermal distortions and dissipate the heat to the building platform [80].

Several support geometries have been proposed [81]. One of the most popular design solutions presented in literature consists of lattice lightweight structures reducing the amount of wasted support material [82–87]. It is also possible to design solid supports in order to reach higher mechanical resistance and thermal conductivity. On the other hand, this solution complicates the support removal phase following the process [88–90].

In order to combine thermal conductivity, resistance and ease of removal, support structures are frequently shaped as a grid of vertical thin walls [87,91,92]. These can consist of different 2D patterns according to the desired mechanical and thermic performances [93].

The present paper adopts thin walls to support the part during the construction. The design method details are presented in Sect. 3.1.

3 Method

The proposed method consists of three main phases, namely the definition of objectives (Sect. 3.2), the build orientation optimisation (Sect. 3.3) and the design of support structures (Sect. 3.1.2).

The first phase is delegated to the user in order to include the specific product requirements within the objective function. On the contrary, the last two phases are automatically carried out by the software.

Figure 1 summarises the steps of the method, which are detailed in the next sections.

The build orientation optimisation includes an estimation of the support structures which are necessary to part building. For this reason, the support design strategy is firstly presented in Sect. 3.1.2. Then, Sect. 3.2 introduces the objective functions optimised through the automated orientation algorithm. Finally, details of the GA-based optimisation are presented in Sect. 3.3.

Fig. 1 Framework of the proposed method

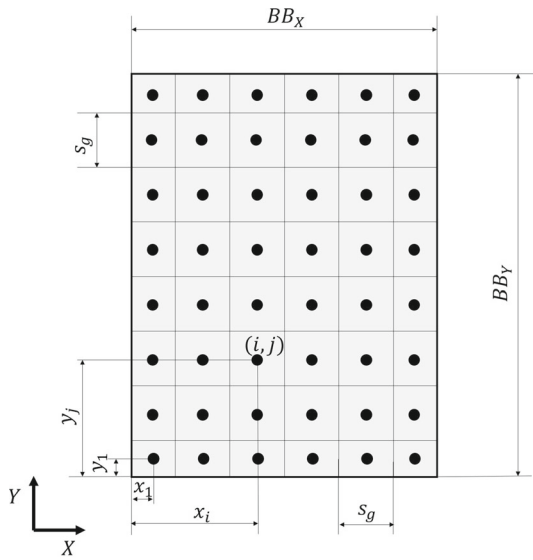
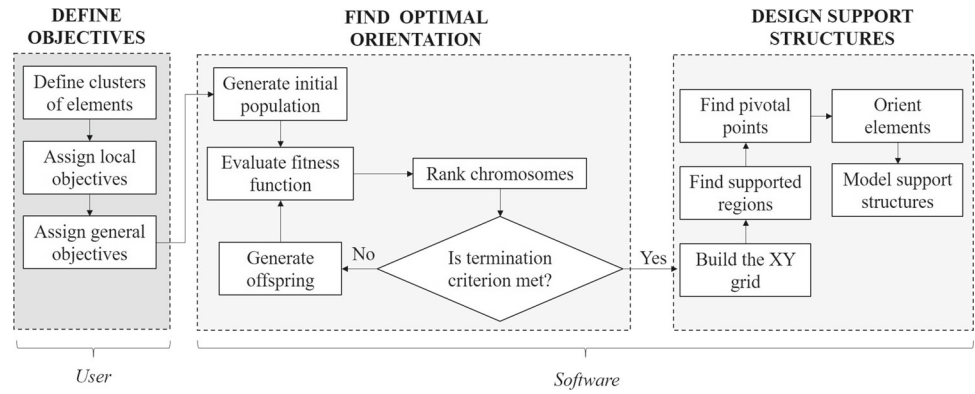


Fig. 2 Planar grid of the part bounding box in XY

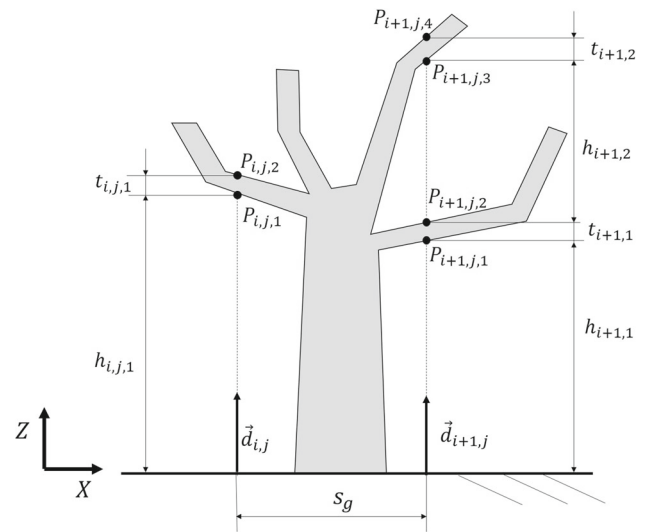


Fig. 3 Intersections of ray casting with the mesh

3.1 Support design

3.1.1 Determination of supported regions

Defining as α_{lim} the minimum angle of a surface to the horizontal plane which allows the self-supporting of the material, the binary value S_i expressing the need for supports for the generic i th triangle can be calculated as in Eq. 1:

$$S_i = 1 - \lceil n_{z,i} + \cos(\alpha_{lim}) \rceil \tag{1}$$

where $n_{z,i}$ is the Z component of the i th triangle normal vector.

The supporting structures are designed through a region-based approach. The dimensions of the bounding box enclosing the part, BB_x , BB_y and BB_z , are firstly calculated.

The XY projection of the bounding box is divided in a grid whose side step is s_g , as shown in Fig. 2.

Vertical rays are cast from the centre of each grid element (highlighted with a dot in Fig. 2). The central coordinates

(x_i, y_j) of the generic grid element (i,j) can be calculated as in Eqs. 2 and 3:

$$x_i = \begin{cases} \frac{1}{2}(BB_x - s_g \lceil \frac{BB_x}{s_g} \rceil) & \text{if } i = 1; \\ BB_x - x_{1,j} & \text{if } i = \lceil \frac{BB_x}{s_g} \rceil; \\ x_{1,j} + (i - 1)s_g & \text{elsewhere;} \end{cases} \tag{2}$$

$$y_j = \begin{cases} \frac{1}{2}(BB_y - s_g \lceil \frac{BB_y}{s_g} \rceil) & \text{if } j = 1; \\ BB_y - y_{1,j} & \text{if } j = \lceil \frac{BB_y}{s_g} \rceil; \\ y_{1,j} + (j - 1)s_g & \text{elsewhere.} \end{cases} \tag{3}$$

A vector $\mathbf{d}_{i,j}$ with origin (x_i, y_j, z_{min}) and direction $(0,0,1)$ is defined for each element (i,j) of the grid, being z_{min} the minimum z coordinate of the bounding box. A ray-casting algorithm [94] is used to check the intersection points $P_{i,j,k}$ of $\mathbf{d}_{i,j}$ with the part, as shown in Fig. 3.

As the part must satisfy the manifold condition, the intersection point $P_{i,j,k}$ lays on a triangle with negative n_z if k is odd and with positive n_z if k is even. The manifold condition also implies that the total number of intersections $P_{i,j,k}$ is

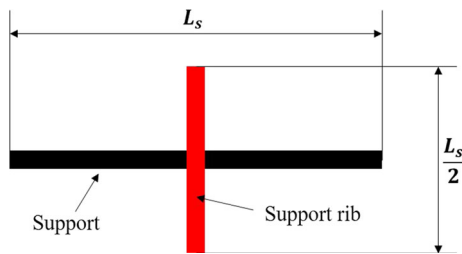


Fig. 4 View of a supporting line and rib in the XY plane

even for every pair (i, j) . The maximum number of intersections found on the grid (i.e. the higher value reached by index k) will be indicated as $N_{max,int}$.

It is then possible to define two three-dimensional matrices with dimensions $[\lceil \frac{BB_x}{s_g} \rceil, \lceil \frac{BB_y}{s_g} \rceil, N_{max,int}]$ that were named H_s and T_s , whose generic elements are defined as in Eqs. 4 and 5, respectively.

$$H_s(i, j, k) = \begin{cases} P_{i,j,2k-1} - P_{i,j,2(k-1)} & \text{if } \exists P_{i,j,2k}; \\ 0 & \text{if } \nexists P_{i,j,2k}; \end{cases} \quad (4)$$

$$T_s(i, j, k) = \begin{cases} P_{i,j,2k} - P_{i,j,2k-1} & \text{if } \exists P_{i,j,2k}; \\ 0 & \text{if } \nexists P_{i,j,2k}. \end{cases} \quad (5)$$

It is important to highlight that the size and values of matrices H_s and T_s vary according to the part orientation.

3.1.2 Design of support structures

As mentioned in Sect. 2.4, thin vertical lines are used as support structures. A transversal rib is added to prevent lateral bending during construction. Figure 4 shows a projection of this structure on the XY plane.

As one single scan line is used for support construction, the actual thickness of the vertical wall depends on a number of parameters, including the scanning speed, the laser power, the reflectivity and the grain size of the powder [95,96].

For each element of a grid in Fig. 2, the necessity of support structures can be determined by means of Eq. 1. The orientation of each wall is chosen in order to minimise the distortion of the part, as described in the following considerations. Indicating as $Tr(P_{i,j,k})$ the triangle on which the intersection point $P_{i,j,k}$ lays, it is possible to define the matrix H_{cp} of dimensions $[\lceil \frac{BB_x}{s_g} \rceil, \lceil \frac{BB_y}{s_g} \rceil, N_{max,int}]$. The generic element $H_{cp}(i, j, k)$ is then calculated as in Eq. 6:

$$H_{cp}(i, j, k) = S_b(Tr(P_{i,j,2k-1})) \times \sum_{l=1}^k [T_s(i, j, l) + H_s(i, j, l)] \quad (6)$$

According to Eq. 6, H_{cp} elements are equal to zero if the region does not require supports and are equal to the height

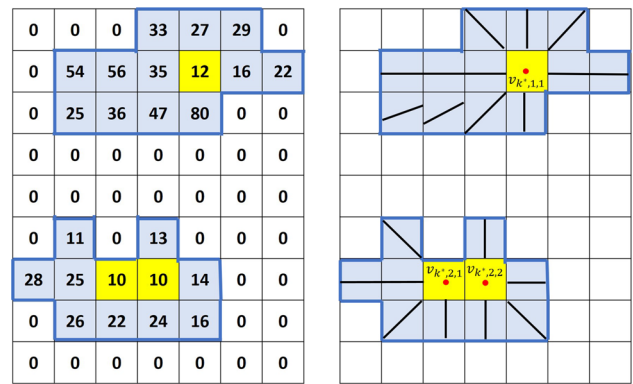


Fig. 5 Example of pivot determination for a given intersection level k^*

of the intersection point from the bottom plane otherwise. Therefore, given a value k^* , referred to in the following as *intersection level*, the two-dimensional matrix $H_{cp}(i, j, k^*)$ is as shown in Fig. 5. In the matrix $H_{cp}(i, j, k^*)$, it is possible to distinguish the cluster of supported elements, coloured in blue in Fig. 5. For each cluster, the minimum values of $H_{cp}(i, j, k^*)$ (highlighted in yellow in Fig. 5) are identified. The corresponding centres of the grid, represented as red dots in Fig. 5, are named *pivotal points* and indicated as $[v_{k^*,h,1}, v_{k^*,h,2}, \dots]$.

For each element (i, j) of the grid, the supporting wall is oriented as the vector connecting the centre of the element (x_i, y_j) with the projection on the XY-plane of the nearest pivotal point $v_{k^*,h,m} = (x_{v^*}, y_{v^*}, z_{v^*})$. The direction vector $\hat{d}_{i,j,k}$ can thus be calculated as in Eq. 7:

$$\hat{d}_{i,j,k} = \left(\frac{x_{v^*} - x_i}{\sqrt{(x_{v^*} - x_i)^2 + (y_{v^*} - y_i)^2}}, \frac{y_{v^*} - y_i}{\sqrt{(x_{v^*} - x_i)^2 + (y_{v^*} - y_i)^2}}, 0 \right) \quad (7)$$

The support design penetrates the point of coordinates (x_i, y_j) and remains inside the grid element, as shown in Fig. 5. The length of the support structure L_s shown in Fig. 4 can be thus calculated as in Eq. 8:

$$L_s(i, j, k) = \max\left(\frac{s_g}{|\hat{d}_{i,j,k} \cdot \hat{X}|}, \frac{s_g}{|\hat{d}_{i,j,k} \cdot \hat{Y}|}\right) \quad (8)$$

where $\hat{X} = \{1, 0, 0\}$ and $\hat{Y} = \{0, 1, 0\}$.

The length of the line is reduced in correspondence to the connection between supports and the part in order to ease the removal of the structures at the end of the process. The transitions between supports and the part are named *teeth* and present the typical shape shown in Fig. 6. The height of the support tooth h_{st} and the aspect ratio α_{ls} between the length of the line L_s and the final length of the tooth L_{se} are used to define the geometry of the teeth.

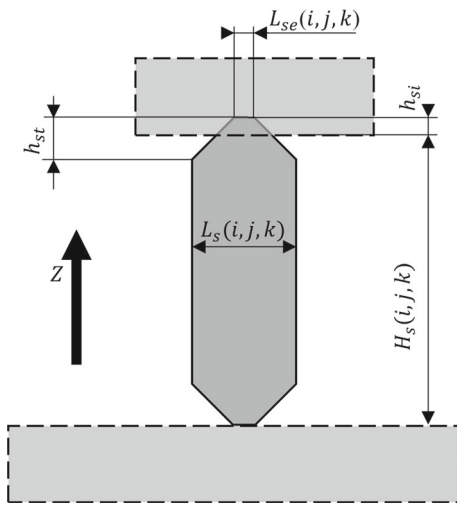


Fig. 6 Schematisation of support wall and connection teeth

The height of the support along the Z direction can be obtained by the matrix H_s calculated in Eq. 4. It is worth mentioning that the actual coordinates of the connection to the part may vary according to the slope of the surface: the ray-casting approach exposed above can be extended to calculate such positions.

The length of support penetration within the part is equal to h_{st} . This has to be compared to the thickness values in the matrix T_s , Eq. 5, in order to prevent part piercing.

A difference between the top and bottom design of teeth may be operated at different levels; as an example, the bottom teeth of the first level (i.e. the connection of the part to the build platform) is often avoided (i.e. $\alpha_{ls} = 1$) in order to improve the resistance, as this region does not affect the surface quality of the part.

3.2 Definition of the objectives

3.2.1 Fitness function

The build orientation optimisation consists in finding the optimal Eulerian angles α_x , α_y and α_z between the coordinate system of the part and the machine one. To achieve this aim, the fitness function $F_f(\alpha_x, \alpha_y, \alpha_z)$ presented in Eq. 9 must be minimised:

$$F_f(\alpha_x, \alpha_y, \alpha_z) = p_t \times w_t + p_v \times w_v + p_d \times w_d + p_r + p_s \quad (9)$$

The notation in Eq. 9 is the following:

- p_b : penalty value of the building time;
- w_t : weight assigned to the building time;
- p_v : penalty value of the support volume;

- w_v : weight the support volume;
- p_d : penalty value of the average distortion;
- w_d : weight assigned to the average distortion;
- $p_r = \frac{1}{N_t} \times \sum_{i=1}^{N_t} p_{r,i} \times w_{r,i}$
- N_t : number of triangles in the mesh;
- $p_{r,i}$: penalty value of the roughness of the i th triangle;
- $w_{r,i}$: weight of the roughness of the i th triangle;
- $p_s = \frac{1}{N_t} \times \sum_{i=1}^{N_t} S_i \times w_{s,i}$
- S_i : presence of supports on the i th triangle;
- $w_{s,i}$: weight of the presence of supports on the i th triangle;

As mentioned, the weights have to be assigned by the user according to the functional requirements of the product. It is important to underline that the weight of the building time, support volume and average distortion are defined on the entire product, whereas $w_{s,i}$ and $w_{r,i}$ are assigned to each triangle so as to better fit the local needs. To simplify the assignment procedure, it is possible to define clusters of elements having the same functional requirements, as shown in the case study of Sect. 4.

Penalty factors p_t , p_v and p_r are real values in the range $[0; 1]$. The calculation of these coefficients is presented in the next sections.

3.2.2 Building time penalty function

As mentioned in Sect. 2.1, the penalty value associated with the building time is estimated based on the maximum height h_{max} along the Z-axis. Obviously, the maximum height depends on the part orientation, i.e. h_{max} is a function of Eulerian angles $(\alpha_x, \alpha_y, \alpha_z)$.

To normalise the value of p_t in the range $]0; 1]$, the maximum height is divided by the diagonal of the bounding box in its original orientation, as shown in Eq. 10:

$$p_t = \frac{h_{max}}{\sqrt{BB_{0x}^2 + BB_{0y}^2 + BB_{0z}^2}} \quad (10)$$

where BB_{0x} , BB_{0y} and BB_{0z} are, respectively, the x, y and z dimensions of the bounding box enclosing the part in its original orientation.

3.2.3 Support volume penalty function

In order to estimate the support mass, the volume of the supported area defined in Sect. 3.1.1 is used. In greater detail, the supported region is calculated by multiplying the area of grid elements in Fig. 2 by the height of the supported region shown in Fig. 6. This approach does not consider the volume variation occurring due to the different orientation of support

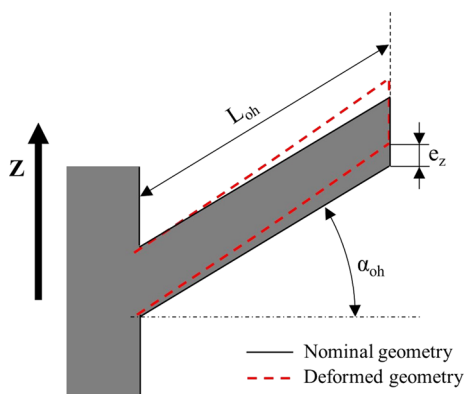


Fig. 7 Schematisation of support wall and connection teeth

structures, as this is supposed to be negligible for the purpose of the comparison.

The volume calculated through this method is then divided by the one of the bounding box enclosing the part in its original orientation, so as to have $p_v \in [0; 1]$. The penalty function of support volume is thus calculated as in Eq. 11:

$$p_v = \frac{\sum_{i=1}^{\lceil \frac{BB_x}{s_g} \rceil} \sum_{j=1}^{\lceil \frac{BB_y}{s_g} \rceil} \sum_{k=1}^{N_{max,int}} H_s(i, j, k) s_g^2}{BB_{0x} BB_{0y} BB_{0z}} \tag{11}$$

3.2.4 Distortion penalty function

The penalty function for accuracy loss is calculated through an estimation of the part distortions induced by the printing process. The estimation is made through a regression of experimental results already published. Unlike FEA simulation [97–99], this approach allows for a fast calculation of the penalty function.

As presented in [100], experimental tests reveal a good correlation between these distortions and the main dimensions of overhangs. In greater detail, the vertical displacement of the overhang e_z depends on the overhang thickness (t_{oh}), inclination (α_{oh}) and length (L_{oh}), as shown in Fig. 7.

Using the definitions given in Sect. 3.1.2, let $[x_p, y_p, z_p]$ be the cartesian coordinates of the generic intersection point $P_{i,j,k}$ and $[x_{v*}, y_{v*}, z_{v*}]$ the ones of the corresponding pivotal point. The equivalent overhang length $L_{oh}(P_{i,j,k})$ and $\alpha_{oh}(P_{i,j,k})$ for the intersection point $P_{i,j,k}$ can thus be calculated as in Eqs. 12 and 13, respectively:

$$L_{oh}(P_{i,j,k}) = \sqrt{(x_p - x_{v*})^2 + (y_p - y_{v*})^2 + (z_p - z_{v*})^2} \tag{12}$$

$$\alpha_{oh}(P_{i,j,k}) = \text{Arctan}\left(\frac{z_p - z_{v*}}{\sqrt{(x_p - x_{v*})^2 + (y_p - y_{v*})^2}}\right) \tag{13}$$

The results in [100] also highlight a pivotal role of the distance d_{sl} between support lines. For the scope of this study, this value is set equal to the cell size, i.e. $d_{sl} = s_g$. Therefore, in the case of austenitic stainless steel, it is possible to estimate the vertical displacement e_z by means of Eq. 14 [100]:

$$e_z(P_{i,j,k}) = -1.89 \times 10^{-1} + 9.9 \times 10^{-4} L_{oh} + 7.31 \times 10^{-2} t_{oh} + 8.56 \times 10^{-4} \alpha_{oh} - 2.345 \times 10^{-1} d + -9.5 \times 10^{-5} L_{oh} + \alpha_{oh} - 3.935 \times 10^{-3} t_{oh} \alpha_{oh} + 5.97 \times 10^{-2} t_{oh} d_{sl} \tag{14}$$

As discussed in [100], Eq. 14 fits experimental results with an adjusted determination coefficient $R_{adj}^2 = 90.02\%$, which is considered sufficient for the scope of this comparison. The relative error $\epsilon(P_{i,j,k})$ for the generic contact point is then obtained dividing the displacement calculated as in Eq. 14 by the height of the overhang along the Z-axis, i.e. as in Eq. 15:

$$\epsilon(P_{i,j,k}) = \frac{e_z(P_{i,j,k})}{L_{oh} \times \text{Sin}(\alpha_{oh})} \tag{15}$$

Finally, the distortion penalty function is obtained by averaging the values of $\epsilon(P_{i,j,k})$ of all the intersection points, as shown in Eq. 16:

$$p_d = \frac{\sum_{i=1}^{\lceil \frac{BB_x}{s_g} \rceil} \sum_{j=1}^{\lceil \frac{BB_y}{s_g} \rceil} \sum_{k=1}^{N_{max,int}} \epsilon(P_{i,j,k})}{\lceil \frac{BB_x}{s_g} \rceil \lceil \frac{BB_y}{s_g} \rceil N_{max,int}} \tag{16}$$

3.2.5 Roughness penalty function

As mentioned in Sect. 2.2, an estimation of PBF part roughness is adopted. This is obtained through the normal component along the Z-axis $N_{z,i}$ of each i th facet.

Particularly, the following considerations are reflected:

- The minimum roughness is achieved for upward-facing elements;
- The roughness decreases with the absolute value of N_z ;
- The roughness is higher on downward-facing elements.

Accordingly, the penalty of roughness for the generic i th triangle is calculated as in Eq. 17:

$$p_{r,i} = (1 - \lfloor \frac{1 + N_{i,z}}{2} \rfloor)(k_1 e^{|N_{i,z}|} + k_2 \lfloor \frac{1 - \text{sign}(N_{i,z})}{2} \rfloor) \tag{17}$$

The coefficients k_1 and k_2 in Eq. 17 are set equal to 0.15 and 0.3, respectively. Figure 8 shows the graph of $p_{r,i}$ as

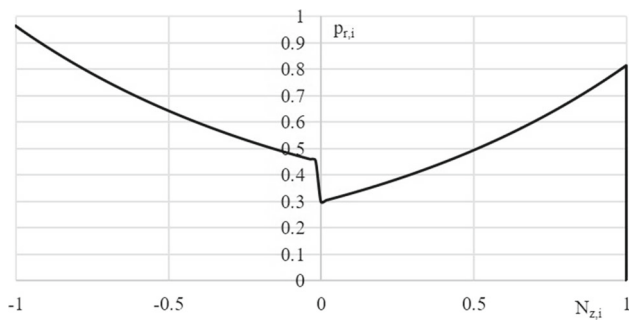


Fig. 8 Roughness penalty $p_{r,i}$ versus z component of normal vector of the i th triangle

function on $N_{i,z}$. As it can be noticed, the trend of roughness reflects the experimental results of the body of research presented in Sect. 2.2.

3.3 Build orientation optimisation

The build orientation optimisation aims at the minimisation of the fitness function in Eq. 9. The G chromosome encodes the Eulerian angles α_x , α_y and α_z as integer values. The minimum rotation is thus equal to 1° . To represent an integer in the range $[0^\circ; 360^\circ]$ as a binary 9 digits are necessary. As a consequence, the chromosome comprises 27 genes.

The crossover operator generates the offspring through a two-point strategy. The splitting points of the crossover correspond to the end of Eulerian angles, i.e. between the 9th and 10th chromosomes and between the 18th and 19th chromosomes.

In order to prevent deadlock in local minima, a flip-bit mutation strategy is included, i.e. each chromosome has a given probability to switch from 0 to 1 and vice versa.

An elitist strategy is applied to select the best chromosomes of each generation, which are the parents of the offspring.

The algorithm is terminated through a stagnation strategy, i.e. when the best value of the fitness function does not decrease after a predetermined number of generations.

The best individual of the last generation is the optimal orientation under the set of requirements defined by the user.

4 Case study

4.1 Model and parameters

A digital model of bottle opener made available on Thingiverse [101] was used for benchmarking the application. The model comprised 16844 triangles with a total volume of 4672 mm^3 .

Two clusters of elements were defined, namely the handle and the opener regions, shown in Fig. 9a, b, respectively.

The coefficients $w_{r,i}$ and $w_{s,i}$ of the elements belonging to cluster 1, namely the handle, were set to 10. Therefore, the objective of the orientation was to avoid support structures and reduce the roughness of this region, so as to ease the following machining operations. In order to limit as much as possible support structures in the opener region, the values $w_{s,i}$ of elements in cluster 2 were equal to 10. As the roughness in this region was assumed not to be relevant, $w_{r,i}$ coefficients were set to 0. $w_{r,i}$ and $w_{s,i}$ of all the elements out of the clusters were also equal to 0.

Three scenarios were tested assigning a different relevance to each aim of the optimisation. Specifically, in the first case, the priority was given to building time, while support volume and accuracy are considered negligible. Then, in the second scenario, the support volume was the priority. Finally, the third case aimed at the minimisation of the part distortion followed by overall roughness. Based on these priorities, the weights of the optimisation were set as summarised in Table 1.

At each iteration of the GA, the number of chromosomes in the population was between 20 and 30. The mutation coefficient of each gene was set equal to 0.3, i.e. each bit had the 30% of probability to switch from 0 to 1 and vice versa after crossover. The GA was terminated when the fitness of the best chromosome did not decrease after 25 iterations.

The part was placed at 5 mm from the base of the platform. The grid side s_g and the limit self-supporting angle were equal to 2 mm and 50° , respectively.

The method was implemented through the C# programming language. GeneticSharp library was used for the implementation of GA functions. Calculations were run on a 32 GB Intel Core i9 - 7920X 2.9 GHz processing unit.

Fig. 9 a Cluster of elements number 1: handle, 2384 facets. b Cluster of elements number 2: Opener, 163 facets

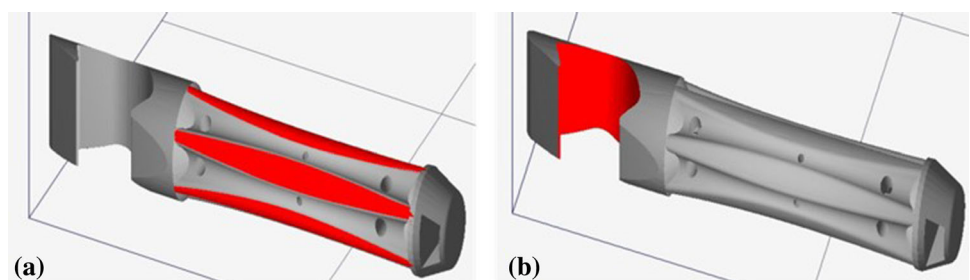


Table 1 Weights used for the different case studies

Case	w_t	w_v	w_d	$w_{r,i}$ (out of clusters)
1	0.8	0.1	0.1	0.0
2	0.1	0.8	0.1	0.0
3	0.1	0.1	0.8	0.5

Table 2 Iterations with improvements of the fitness function for Case 1

Iter.	F_f	p_s	p_r	p_d	p_t	p_v
1	1.562	0.091	0.716	0.177	0.891	0.245
13	1.498	0.024	0.699	0.258	0.905	0.251
14	1.483	0.283	0.949	0.495	0.203	0.393
19	1.482	0.287	0.949	0.669	0.179	0.357
23	1.476	0.282	0.948	0.328	0.216	0.408
24	1.473	0.278	0.949	0.468	0.200	0.388

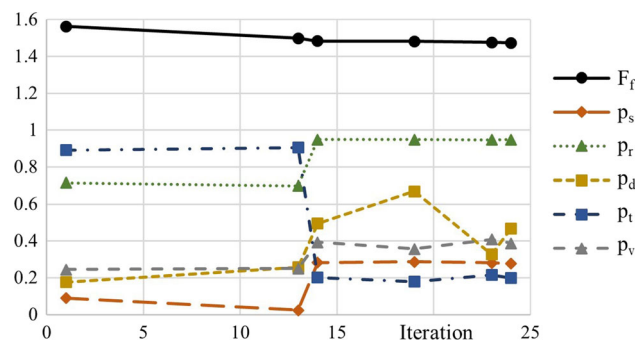


Fig. 10 Fitness and penalty functions over iterations for Case 1

Autodesk NetFabb @post processor for SLM 280 HL @LPBF machine was used to estimate the building time of the solutions. In order to calculate the support structures volume, the width of the single line scan was assumed to be 0.3 mm.

4.2 Results

4.2.1 Case 1

The optimisation lasted 7 min and 1 s. The optimal solution was reached after 48 iterations. The values of fitness and penalty functions for significant iterations (namely the ones where an improvement in F_f is observed) are summarised in Table 2 and graphically shown in Fig. 10.

The Eulerian angles corresponding to the optimal solutions were $\alpha_x = 0^\circ$, $\alpha_y = 184^\circ$ and $\alpha_z = 138^\circ$. The final orientation corresponding to these angles is shown in Fig. 11.

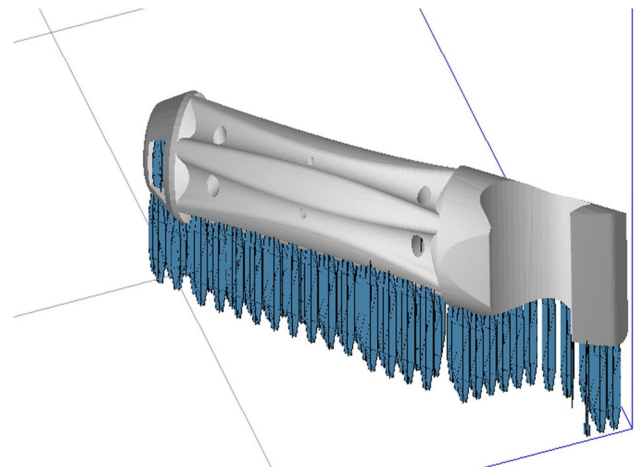


Fig. 11 Optimal orientation found for Case 1

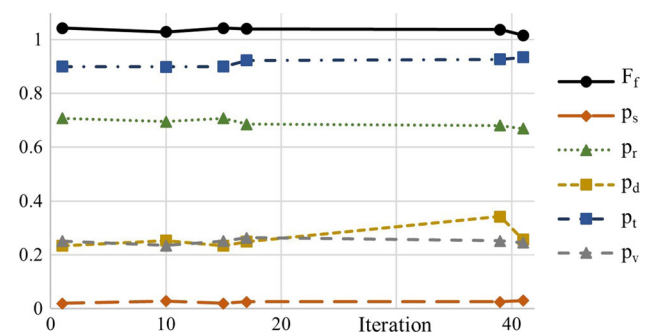


Fig. 12 Fitness and penalty functions over iterations for Case 2

The estimated building time of this solution is 2 h 26 min and 38 s. The volume of support structures is equal to 737.8 mm³.

4.2.2 Case 2

The optimisation lasted 9 min and 27 s. The optimal solution was reached after 65 iterations. The most relevant iterations are reported in Table 2 and Fig. 12.

The Eulerian angles corresponding to the optimal solutions were $\alpha_x = 20^\circ$, $\alpha_y = 252^\circ$ and $\alpha_z = 219^\circ$. Such orientation is shown in Fig. 12.

The estimated building time of this solution is 7 h 34 min and 48 s, while the volume of support structures is equal to 246.4 mm³ (Fig. 13, Table 3).

4.2.3 Case 3

The optimisation lasted 7 min and 7 s. The optimal solution was reached after 48 iterations. The most relevant iterations are reported in Table 4 and Fig. 14.

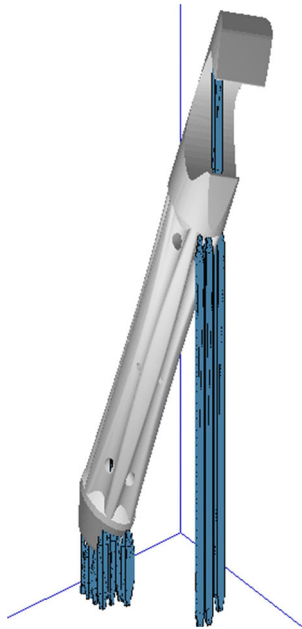


Fig. 13 Optimal orientation found for Case 2

Table 3 Iterations with improvements of the fitness function for Case 2

Iter.	F_f	p_s	p_r	p_d	p_t	p_v
1	1.044	0.020	0.708	0.235	0.900	0.252
10	1.029	0.030	0.695	0.254	0.899	0.236
15	1.044	0.020	0.708	0.235	0.900	0.252
17	1.041	0.026	0.686	0.250	0.923	0.265
39	1.038	0.027	0.681	0.344	0.927	0.253
41	1.017	0.031	0.669	0.258	0.934	0.246

Table 4 Iterations with improvements of the fitness function for Case 3

Iter.	F_f	p_s	p_r	p_d	p_t	p_v
1	1.267	0.167	0.898	0.108	0.931	0.223
3	1.260	0.139	0.911	0.120	0.924	0.220
6	1.246	0.091	0.942	0.126	0.879	0.240
11	1.225	0.168	0.879	0.078	0.931	0.223
16	1.205	0.142	0.885	0.080	0.926	0.215
24	1.203	0.161	0.859	0.081	0.947	0.235

The Eulerian angles corresponding to the optimal solutions were $\alpha_x = 355^\circ$, $\alpha_y = 102^\circ$ and $\alpha_z = 203^\circ$. Such orientation is shown in Fig. 15.

The estimated building time of this solution is 7 h 40 min and 8 s, while the volume of support structures is equal to 339.5 mm^3 .

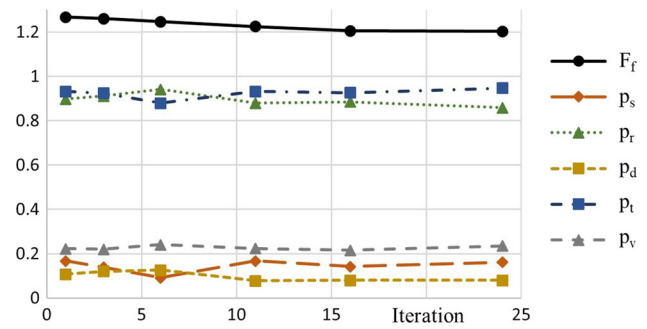


Fig. 14 Fitness and penalty functions over iterations for Case 3

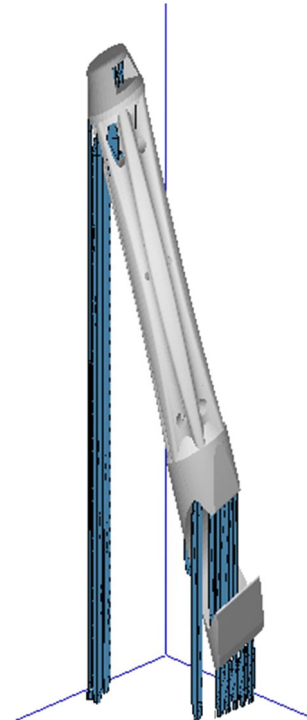


Fig. 15 Optimal orientation found for Case 3

4.3 Discussion

The results presented in the previous section show that the algorithm converged to a minimum in all the analysed case studies. The total number of iterations and the computation time demonstrated the rapidity of the proposed approach when applied to the benchmark geometry. Nonetheless, an increase in computational cost is expected in the case of more complex meshes, i.e. increasing the number of facets.

It is worth remarking that different trends are observed for penalty functions depending on the assigned weights while the global fitness function F_f decrease through iterations. For example, Fig. 10 and Table 2 show that in Case 1 a sharp

increase in support volume, part distortion and accuracy is observed at the 14th iteration. This increase is considered acceptable by the algorithm due to the concomitant reduction of the building time, which is the major aim of this scenario.

Similarly, in the second scenario both p_t and p_d increase moving from the first to the last iteration in favour of a reduction in p_v . This is coherent with the values of w_t , w_d and w_v set for this case.

It is possible to observe that the accuracy penalty function of Case 1 is far higher than the one of Case 2. In fact, the solution proposed for Case 1 is expected to suffer from severe curling and distortion. This is also confirmed by the fact that the optimal solution found in Case 3, where maximum priority is given to the accuracy, looks more similar to the one proposed for Case 2 (see and compare Figs. 13 and 15). Also, in Case 3 a reduction of roughness penalty function p_r between the first and the last iterations is observed. This demonstrates the ability of the proposed method to meet also the second priority of this case scenario.

As can be seen, all the solutions admitted some support structures on elements belonging to cluster 1. It is worth underlining that, due to the geometry of the part, it is not possible to completely avoid supports in this region. In the last two scenarios, a small number of supports was also placed in the opener region, i.e. cluster 2. Therefore the algorithm proposed a compromise solution balancing local and global requirements.

In a real application, the user might evaluate the features of the proposed solution and eventually modify the definition of requirements. This gives the opportunity to iteratively refine the solution through a man-machine interaction.

5 Conclusions

The part build orientation and the design of support structures are crucial steps to the success of the LPBF process. A new method to aid these steps through software was presented in this study. Unlike in previous methods, simultaneous optimisation of part orientation and support design is carried out.

The proposed approach starts from a set of local and global objectives defined by the user. To optimise these aims, comparative functions assessing the build time, support volume, roughness and position of support structures were defined. These functions describe the effects of part orientation while preserving a low computational cost. It was shown how the proposed formulation allows for manual customisation of the objective function based on specific design requirements, thus enhancing the interaction between human and software capabilities.

The application of the proposed approach to a real product reached pseudo optimal solutions in a small number of iterations and within less than 10 min. Also, these solutions

efficiently interpreted the objectives imposed by the user to part orientation. In greater detail, solution 1 allowed for saving 5 h and 13 min with respect to solution 2, i.e. 68.1% of the entire building time. On the other hand, the volume of support structures was reduced by 491.4 mm³ through the adoption of solutions 2. Solution 3 was used to demonstrate the effectiveness of the proposed method in minimising surface roughness and part distortion.

The proposed solution interprets some basic user requirements concerning the building time, support structures and surface roughness, and outputs the oriented part and supports. Therefore, this system is an intuitive and efficient aid to the LPBF process preparation.

Acknowledgements The authors would like to thank the MIUR (Italian Ministry of University and Research) for funding support.

Data availability Please, contact the authors if you are interested in the raw data required to reproduce these findings that are available to download.

Declarations

Competing interest The authors declare that they have no known competing financial interests or personal relationships that could have appeared to influence the work reported in this paper.

References

1. Ngo, T.D., Kashani, A., Imbalzano, G., Nguyen, K.T., Hui, D.: Additive manufacturing (3D printing): a review of materials, methods, applications and challenges. *Compos. B Eng.* **143**(February), 172 (2018). <https://doi.org/10.1016/j.compositesb.2018.02.012>
2. Ali, M.H., Batai, S., Sarbassov, D.: 3D printing: a critical review of current development and future prospects. *Rapid Prototyp. J.* **25**(6), 1108 (2019). <https://doi.org/10.1108/RPJ-11-2018-0293>
3. Briard, T., Segonds, F., Zamariola, N.: G-DfAM: a methodological proposal of generative design for additive manufacturing in the automotive industry. *Int. J. Interact. Des. Manuf.* **14**(3), 875 (2020). <https://doi.org/10.1007/s12008-020-00669-6>
4. Haghdad, N., Laleh, M., Moyle, M., Primig, S.: Additive manufacturing of steels: a review of achievements and challenges. *J. Mater. Sci.* (2020). <https://doi.org/10.1007/s10853-020-05109-0>
5. Bhavar, V., Kattire, P., Patil, V., Khot, S., Gujar, K., Singh, R.: Additive Manufacturing Handbook: Product Development for the Defense Industry (September), p. 251. CRC Press, Boca Raton (2017). <https://doi.org/10.1201/9781315119106>
6. Zitelli, C., Folgarait, P., Di Schino, A.: Laser powder bed fusion of stainless steel grades: a review. *Metals* (2019). <https://doi.org/10.3390/met9070731>
7. Vock, S., Klöden, B., Kirchner, A., Weißgärber, T., Kieback, B.: Powders for powder bed fusion: a review. *Prog. Addit. Manuf.* **4**(4), 383 (2019). <https://doi.org/10.1007/s40964-019-00078-6>
8. Singh, R., Gupta, A., Tripathi, O., Srivastava, S., Singh, B., Awasthi, A., Rajput, S.K., Sonia, P., Singhal, P., Saxena, K.K.: Powder bed fusion process in additive manufacturing: an overview. *Mater. Today Proc.* **26**, 3058 (2019). <https://doi.org/10.1016/j.matpr.2020.02.635>

9. Moshiri, M., Candeo, S., Carmignato, S., Mohanty, S., Tosello, G.: Benchmarking of laser powder bed fusion machines. *J. Manuf. Mater. Process.* **3**, 85 (2019). <https://doi.org/10.3390/jmmp3040085>
10. Khorasani, A.M., Gibson, I., Veetil, J.K., Ghasemi, A.H.: A review of technological improvements in laser-based powder bed fusion of metal printers. *Int. J. Adv. Manuf. Technol.* **108**(1–2), 191 (2020). <https://doi.org/10.1007/s00170-020-05361-3>
11. Samantaray, M., Thatoi, D.N., Sahoo, S.: Modeling and optimization of process parameters for laser powder bed fusion of AlSi10Mg alloy. *Lasers Manuf. Mater. Process.* **6**(4), 356 (2019). <https://doi.org/10.1007/s40516-019-00099-7>
12. Oliveira, J.P., LaLonde, A.D., Ma, J.: Processing parameters in laser powder bed fusion metal additive manufacturing. *Mater. Des.* **193**, 1 (2020). <https://doi.org/10.1016/j.matdes.2020.108762>
13. Nandy, J., Sarangi, H., Sahoo, S.: A review on direct metal laser sintering: process features and microstructure modeling. *Lasers Manuf. Mater. Process.* (2019). <https://doi.org/10.1007/s40516-019-00094-y>
14. Yao, Y., Wang, K., Wang, X., Li, L., Cai, W., Kelly, S., Esparagoza, N., Rosser, M., Yan, F.: Microstructural heterogeneity and mechanical anisotropy of 18Ni-330 maraging steel fabricated by selective laser melting: the effect of build orientation and height. *J. Mater. Res.* **35**(15), 2065 (2020). <https://doi.org/10.1557/jmr.2020.126>
15. Gor, M., Soni, H., Wankhede, V., Sahlot, P., Grzelak, K., Szachgluchowicz, I., Kluczyński, J.: A critical review on effect of process parameters on mechanical and microstructural properties of powder-bed fusion additive manufacturing of ss316L. *Materials* (2021). <https://doi.org/10.3390/ma14216527>
16. Kumar, M.S., Javidrad, H.R., Shanmugam, R., Ramoni, M., Adedirani, A.A., Pruncu, C.I.: Impact of print orientation on morphological and mechanical properties of L-PBF based AlSi7Mg parts for aerospace applications. *Silicon* (2021). <https://doi.org/10.1007/s12633-021-01474-w>
17. Piscopo, G., Salmi, A., Atzeni, E.: On the quality of unsupported overhangs produced by laser powder bed fusion. *Int. J. Manuf. Res.* **14**(2), 198 (2019). <https://doi.org/10.1504/IJMR.2019.100012>
18. Zhang, Y., Yang, S., Zhao, Y.F.: Manufacturability analysis of metal laser-based powder bed fusion additive manufacturing—a survey. *Int. J. Adv. Manuf. Technol.* **110**(1–2), 57 (2020). <https://doi.org/10.1007/s00170-020-05825-6>
19. C.J. Montgomery, B.S.M. Engineering, M.S.M. Engineering (December) (2017)
20. Paudel, B.J., Thompson, S.M.: Solid Freeform Fabrication 2019: Proceedings of the 30th Annual International Solid Freeform Fabrication Symposium—An Additive Manufacturing Conference (2019)
21. Kozior, T., Bochnia, J.: The influence of printing orientation on surface texture parameters in powder bed fusion technology with 316L steel. *Micromachines* (2020). <https://doi.org/10.3390/MII1070639>
22. Di Angelo, L., Di Stefano, P., Guardiani, E.: Search for the optimal build direction in additive manufacturing technologies: a review. *J. Manuf. Mater. Process.* **4**(3), 71 (2020). <https://doi.org/10.3390/jmmp4030071>
23. Cloots, M., Spierings, A., Wegener, K.: Solid Freeform Fabrication Symposium, pp. 631–643 (2013)
24. Alexander, P., Allen, S., Dutta, D.: Part orientation and build cost determination in layered manufacturing. *Comput. Aided Des.* **30**(5), 343 (1998). [https://doi.org/10.1016/S0010-4485\(97\)00083-3](https://doi.org/10.1016/S0010-4485(97)00083-3)
25. Costabile, G., Fera, M., Fruggiero, F., Lambiase, A., Pham, D.: Cost models of additive manufacturing: a literature review. *Int. J. Ind. Eng. Comput.* **8**(2), 263 (2016). <https://doi.org/10.5267/j.ijiec.2016.9.001>
26. Baumers, M., Tuck, C., Wildman, R., Ashcroft, I., Rosamond, E., Hague, R.: Transparency built-in: energy consumption and cost estimation for additive manufacturing Baumers et al. energy and cost estimation for additive manufacturing. *J. Ind. Ecol.* **17**(3), 418 (2013). <https://doi.org/10.1111/j.1530-9290.2012.00512.x>
27. Piili, H., Happonen, A., Väistö, T., Venkataramanan, V., Partanen, J., Salminen, A.: Cost estimation of laser additive manufacturing of stainless steel. *Phys. Procedia* **78**(August), 388 (2015). <https://doi.org/10.1016/j.phpro.2015.11.053>
28. Pham, D.T., Wang, X.: Prediction and reduction of build times for the selective laser sintering process. *Proc. Inst. Mech. Eng. Part B J. Eng. Manuf.* **214**(6), 425 (2000). <https://doi.org/10.1243/0954405001517739>
29. Giannatsis, J., Dedoussis, V., Laios, L.: A study of the build-time estimation problem for Stereolithography systems. *Robot. Comput. Integr. Manuf.* **17**(4), 295 (2001). [https://doi.org/10.1016/S0736-5845\(01\)00007-2](https://doi.org/10.1016/S0736-5845(01)00007-2)
30. Rickenbacher, L., Spierings, A., Wegener, K.: An integrated cost-model for selective laser melting (SLM). *Rapid Prototyp. J.* **19**(3), 208 (2013). <https://doi.org/10.1108/13552541311312201>
31. Di Angelo, L., Di Stefano, P.: A neural network-based build time estimator for layer manufactured objects. *Int. J. Adv. Manuf. Technol.* **57**(1–4), 215 (2011). <https://doi.org/10.1007/s00170-011-3284-8>
32. Calignano, F.: Investigation of the accuracy and roughness in the laser powder bed fusion process. *Virtual Phys. Prototyp.* **13**(2), 97 (2018). <https://doi.org/10.1080/17452759.2018.1426368>
33. Ali, U., Fayazfar, H., Ahmed, F., Toyserkani, E.: Internal surface roughness enhancement of parts made by laser powder-bed fusion additive manufacturing. *Vacuum* (2020). <https://doi.org/10.1016/j.vacuum.2020.109314>
34. Dmitriyev, T., Manakov, S.: Digital modeling accuracy of direct metal laser sintering process. *Eurasian Chem. Technol. J.* **22**(2), 123 (2020). <https://doi.org/10.18321/ectj959>
35. Strano, G., Hao, L., Everson, R.M., Evans, K.E.: Surface roughness analysis, modelling and prediction in selective laser melting. *J. Mater. Process. Technol.* **213**(4), 589 (2013). <https://doi.org/10.1016/j.jmatprotec.2012.11.011>
36. Wang, D., Liu, Y., Yang, Y., Xiao, D.: Theoretical and experimental study on surface roughness of 316L stainless steel metal parts obtained through selective laser melting. *Rapid Prototyp. J.* **22**(4), 706 (2016). <https://doi.org/10.1108/RPJ-06-2015-0078>
37. Fox, J.C., Moylan, S.P., Lane, B.M.: Effect of process parameters on the surface roughness of overhanging structures in laser powder bed fusion additive manufacturing. *Procedia CIRP* **45**, 131 (2016). <https://doi.org/10.1016/j.procir.2016.02.347>
38. Guo, C., Li, S., Shi, S., Li, X., Hu, X., Zhu, Q., Ward, R.M.: Effect of processing parameters on surface roughness, porosity and cracking of as-built IN738LC parts fabricated by laser powder bed fusion. *J. Mater. Process. Technol.* **285**(December 2019), 116788 (2020). <https://doi.org/10.1016/j.jmatprotec.2020.116788>
39. Rott, S., Ladewig, A., Friedberger, K., Casper, J., Full, M., Schleifenbaum, J.H.: Surface roughness in laser powder bed fusion—interdependency of surface orientation and laser incidence. *Addit. Manuf.* (2020). <https://doi.org/10.1016/j.addma.2020.101437>

40. Frank, D., Fadel, G.: Expert system-based selection of the preferred direction of build for rapid prototyping processes. *J. Intell. Manuf.* **6**(5), 339 (1995). <https://doi.org/10.1007/BF00124677>
41. Lan, P.T., Chou, S.Y., Chen, L.L., Gemmill, D.: Determining fabrication orientations for rapid prototyping with stereolithography apparatus. *CAD Comput. Aided Des.* **29**(1), 53 (1997). [https://doi.org/10.1016/S0010-4485\(96\)00049-8](https://doi.org/10.1016/S0010-4485(96)00049-8)
42. Leutenecker-Twelsiek, B., Klahn, C., Meboldt, M.: Considering part orientation in design for additive manufacturing. *Procedia CIRP* **50**, 408 (2016). <https://doi.org/10.1016/j.procir.2016.05.016>
43. Masood, S.H., Rattanawong, W., Iovenitti, P.: A generic algorithm for a best part orientation system for complex parts in rapid prototyping. *J. Mater. Process. Technol.* **139**(1–3 SPEC), 110 (2003). [https://doi.org/10.1016/S0924-0136\(03\)00190-0](https://doi.org/10.1016/S0924-0136(03)00190-0)
44. Singhal, S.K., Jain, P.K., Pandey, P.M., Nagpal, A.K.: Optimum part deposition orientation for multiple objectives in SL and SLS prototyping. *Int. J. Prod. Res.* **47**(22), 6375 (2009). <https://doi.org/10.1080/00207540802183661>
45. Morgan, H.D., Cherry, J.A., Jonnalagadda, S., Ewing, D., Sienz, J.: Part orientation optimisation for the additive layer manufacture of metal components. *Int. J. Adv. Manuf. Technol.* **86**(5–8), 1679 (2016). <https://doi.org/10.1007/s00170-015-8151-6>
46. Nezhad, A.S., Vatani, M., Barazandeh, F., Rahimi, A.R.: Proceedings of the 9th WSEAS International Conference on Simulation, Modelling and Optimization, SMO '09, 5th WSEAS International Symposium on Grid Computing, Proceedings of the 5th WSEAS International Symposium on Digital Libraries, Proceedings of the 5th WSEAS International Symposium on Data Mining, pp. 36–40 (2009)
47. Matos, M.A., Rocha, A.M.A., Costa, L.A., Pereira, A.I.: Lecture Notes in Computer Science (Including subseries Lecture Notes in Artificial Intelligence and Lecture Notes in Bioinformatics), 11621 LNCS, p. 261 (2019). <https://doi.org/10.1007/978-3-030-24302-9>
48. Qin, Y., Qi, Q., Scott, P.J., Jiang, X.: Determination of optimal build orientation for additive manufacturing using Muirhead mean and prioritised average operators. *J. Intell. Manuf.* **30**(8), 3015 (2019). <https://doi.org/10.1007/s10845-019-01497-6>
49. Zhang, Y., De Backer, W., Harik, R., Bernard, A.: Build orientation determination for multi-material deposition additive manufacturing with continuous fibers. *Procedia CIRP* **50**, 414 (2016). <https://doi.org/10.1016/j.procir.2016.04.119>
50. Khodaygan, S., Golmohammadi, A.H.: Multi-criteria optimization of the part build orientation (PBO) through a combined meta-modeling/NSGAII/TOPSIS method for additive manufacturing processes. *Int. J. Interact. Des. Manuf.* **12**(3), 1071 (2018). <https://doi.org/10.1007/s12008-017-0443-7>
51. Mele, M., Campana, G.: Sustainability-driven multi-objective evolutionary orienting in additive manufacturing. *Sustain. Prod. Consum.* **23**, 138 (2020). <https://doi.org/10.1016/j.spc.2020.05.004>
52. Huang, R., Dai, N., Cheng, X.: Build orientation optimization for lightweight lattice parts production in selective laser melting by using a multicriteria genetic algorithm. *J. Mater. Res.* **35**(15), 2046 (2020). <https://doi.org/10.1557/jmr.2020.124>
53. Das, P., Chandran, R., Samant, R., Anand, S.: Optimum part build orientation in additive manufacturing for minimizing part errors and support structures. *Procedia Manuf.* **1**, 343 (2015). <https://doi.org/10.1016/j.promfg.2015.09.041>
54. Ga, B., Gardan, N., Wahu, G.: Methodology for part building orientation in additive manufacturing. *Comput. Aided Des. Appl.* **16**(1), 113 (2018). <https://doi.org/10.14733/cadaps.2019.113-128>
55. Golmohammadi, A.H., Khodaygan, S.: A framework for multi-objective optimisation of 3D part-build orientation with a desired angular resolution in additive manufacturing processes. *Virtual Phys. Prototyp.* **14**(1), 19 (2019). <https://doi.org/10.1080/17452759.2018.1526622>
56. Mele, M., Campana, G., Monti, G.L.: Intelligent orientation of parts based on defect prediction in multi jet fusion process. *Prog. Addit. Manuf.* **6**(4), 841 (2021). <https://doi.org/10.1007/s40964-021-00199-x>
57. Thrimurthulu, K., Pandey, P.M., Reddy, N.V.: Optimum part deposition orientation in fused deposition modeling. *Int. J. Mach. Tools Manuf.* **44**(6), 585 (2004). <https://doi.org/10.1016/j.ijmachtools.2003.12.004>
58. Canellidis, V., Giannatsis, J., Dedoussis, V.: Genetic-algorithm-based multi-objective optimization of the build orientation in stereolithography. *Int. J. Adv. Manuf. Technol.* **45**(7–8), 714 (2009). <https://doi.org/10.1007/s00170-009-2006-y>
59. Phatak, A.M., Pande, S.S.: Optimum part orientation in Rapid Prototyping using genetic algorithm. *J. Manuf. Syst.* **31**(4), 395 (2012). <https://doi.org/10.1016/j.jmsy.2012.07.001>
60. Brika, S.E., Zhao, Y.F., Brochu, M., Mezzetta, J.: Multi-objective build orientation optimization for powder bed fusion by laser. *J. Manuf. Sci. Eng. Trans. ASME* (2017). <https://doi.org/10.1115/1.4037570>
61. Mele, M., Campana, G., Lenzi, F., Cimatti, B.: In: *Procedia Manufacturing* vol. 33, pp. 145–152 (2019). <https://doi.org/10.1016/j.promfg.2019.04.019>. <https://www.scopus.com/inward/record.uri?eid=2-s2.0-85068581736&doi=10.1016%2Fj.promfg.2019.04.019&partnerID=40&md5=7db0005b2d50ab61975e9a33c77573a1>
62. Goguelin, S., Dhokia, V., Flynn, J.M.: Bayesian optimisation of part orientation in additive manufacturing. *Int. J. Comput. Integr. Manuf.* **34**(12), 1263 (2021). <https://doi.org/10.1080/0951192X.2021.1972466>
63. Matos, M.A., Rocha, A.M.A., Costa, L.A.: Many-objective optimization of build part orientation in additive manufacturing. *Int. J. Adv. Manuf. Technol.* **112**(3–4), 747 (2021). <https://doi.org/10.1007/s00170-020-06369-5>
64. Reichwein, J., Kirchner, E.: Part orientation and separation to reduce process costs in additive manufacturing. *Proc. Des. Soc.* **1**(August), 2399 (2021). <https://doi.org/10.1017/pds.2021.501>
65. Subbaian Kaliamoorthy, P., Subbiah, R., Bensingh, J., Kader, A., Nayak, S.: Benchmarking the complex geometric profiles, dimensional accuracy and surface analysis of printed parts. *Rapid Prototyp. J.* **26**(2), 319 (2020). <https://doi.org/10.1108/RPJ-01-2019-0024>
66. Zhou, Y., Ning, F.: Build orientation effect on geometric performance of curved-surface 316L stainless steel parts fabricated by selective laser melting. *J. Manuf. Sci. Eng. Trans. ASME* **142**(12), 1 (2020). <https://doi.org/10.1115/1.4047624>
67. Sahoo, S.: Characterization of effect of support structures in laser additive manufacturing of stainless steel. *J. Laser Appl.* **33**(3), 32011 (2021)
68. Nandy, J., Sahoo, S., Sarangi, H., Sabat, R.K.: Evaluation of structural and mechanical properties of high strength aluminum alloy components fabricated using laser powder bed fusion process. *J. Laser Appl.* **33**(3), 32009 (2021)
69. Dareh Baghi, A., Nafisi, S., Hashemi, R., Ebendorff-Heidepriem, H., Ghomashchi, R.: Experimental realisation of build orientation effects on the mechanical properties of truly as-built Ti–6Al–4V SLM parts. *J. Manuf. Process.* **64**(November 2020), 140 (2021). <https://doi.org/10.1016/j.jmapro.2021.01.027>

70. AlRedha, S., Shterenlikht, A., Mostafavi, M., Van Gelderen, D., Lopez-Botello, O.E., Reyes, L.A., Zambrano, P., Garza, C.: Effect of build orientation on fracture behaviour of AlSi10Mg produced by selective laser melting. *Rapid Prototyp. J.* **27**(1), 112 (2021). <https://doi.org/10.1108/RPJ-02-2020-0041>
71. Wang, C.G., Zhu, J.X., Wang, G.W., Qin, Y., Sun, M.Y., Yang, J.L., Shen, X.F., Huang, S.K.: Effect of building orientation and heat treatment on the anisotropic tensile properties of AlSi10Mg fabricated by selective laser melting. *J. Alloys Compd.* (2022). <https://doi.org/10.1016/j.jallcom.2021.162665>
72. Bogojevic, N., Ciric-Kostic, S., Vranić, A., Olmi, G., Crococolo, D.: *Lecture Notes in Mechanical Engineering* (2020)
73. Pellizzari, M., AlMangour, B., Benedetti, M., Furlani, S., Grzesiak, D., Deirmina, F.: Effects of building direction and defect sensitivity on the fatigue behavior of additively manufactured H13 tool steel. *Theor. Appl. Fract. Mech.* (2020). <https://doi.org/10.1016/j.tafmec.2020.102634>
74. Paul, R., Anand, S.: Optimal part orientation in rapid manufacturing process for achieving geometric tolerances. *J. Manuf. Syst.* **30**(4), 214 (2011). <https://doi.org/10.1016/j.jmsy.2011.07.010>
75. Moroni, G., Syam, W.P., Petrò, S.: Functionality-based part orientation for additive manufacturing. *Procedia CIRP* **36**, 217 (2015). <https://doi.org/10.1016/j.procir.2015.01.015>
76. Qin, Y., Qi, Q., Shi, P., Scott, P.J., Jiang, X.: Automatic generation of alternative build orientations for laser powder bed fusion based on facet clustering. *Virtual Phys. Prototyp.* **15**(3), 307 (2020). <https://doi.org/10.1080/17452759.2020.1756086>
77. Qin, Y., Qi, Q., Shi, P., Scott, P.J., Jiang, X.: Status, issues, and future of computer-aided part orientation for additive manufacturing. *Int. J. Adv. Manuf. Technol.* **115**(5–6), 1295 (2021). <https://doi.org/10.1007/s00170-021-06996-6>
78. Samant, R., Ranjan, R., Mhapsekar, K., Anand, S.: Octree data structure for support accessibility and removal analysis in additive manufacturing. *Addit. Manuf.* **22**(November 2017), 618 (2018). <https://doi.org/10.1016/j.addma.2018.05.031>
79. Mirzendehtdel, A.M., Behandish, M., Nelaturi, S.: Optimizing build orientation for support removal using multi-axis machining. *Comput. Graph. (Pergamon)* **99**, 247 (2021). <https://doi.org/10.1016/j.cag.2021.07.011>
80. Zeng, K., Pal, D., Teng, C., Stucker, B.E.: Evaluations of effective thermal conductivity of support structures in selective laser melting. *Addit. Manuf.* **6**, 67 (2015). <https://doi.org/10.1016/j.addma.2015.03.004>
81. Jiang, J., Stringer, J., Xu, X., Zheng, P.: A benchmarking part for evaluating and comparing support structures of additive manufacturing. In: *Proceedings of the International Conference on Progress in Additive Manufacturing*, vol. 2018 (June), p. 196 (2018). <https://doi.org/10.25341/D42G6H>
82. Hussein, A., Hao, L., Yan, C., Everson, R., Young, P.: Advanced lattice support structures for metal additive manufacturing. *J. Mater. Process. Technol.* **213**(7), 1019 (2013). <https://doi.org/10.1016/j.jmatprotec.2013.01.020>
83. Strano, G., Hao, L., Everson, R.M., Evans, K.E.: A new approach to the design and optimisation of support structures in additive manufacturing. *Int. J. Adv. Manuf. Technol.* **66**(9–12), 1247 (2013). <https://doi.org/10.1007/s00170-012-4403-x>
84. Vaidya, R., Anand, S.: Optimum support structure generation for additive manufacturing using unit cell structures and support removal constraint. *Procedia Manuf.* **5**, 1043 (2016). <https://doi.org/10.1016/j.promfg.2016.08.072>
85. Vaissier, B., Pernot, J.P., Chougrani, L., Véron, P.: Genetic-algorithm based framework for lattice support structure optimization in additive manufacturing. *CAD Comput. Aided Des.* **110**, 11 (2019). <https://doi.org/10.1016/j.cad.2018.12.007>
86. Maconachie, T., Leary, M., Lozanovski, B., Zhang, X., Qian, M., Faruque, O., Brandt, M.: SLM lattice structures: properties, performance, applications and challenges. *Mater. Desi.* (2019). <https://doi.org/10.1016/j.matdes.2019.108137>
87. Liang, X., Dong, W., Hinnebusch, S., Chen, Q., Tran, H.T., Lemon, J., Cheng, L., Zhou, Z., Hayduke, D., To, A.C.: Inherent strain homogenization for fast residual deformation simulation of thin-walled lattice support structures built by laser powder bed fusion additive manufacturing. *Addit. Manuf.* **32**, 1 (2020). <https://doi.org/10.1016/j.addma.2020.101091>
88. Gan, M.X., Wong, C.H.: Practical support structures for selective laser melting. *J. Mater. Process. Technol.* **238**, 474 (2016). <https://doi.org/10.1016/j.jmatprotec.2016.08.006>
89. Ceccanti, F., Giorgetti, A., Citti, P.: A support structure design strategy for laser powder bed fused parts. *Procedia Struct. Integr.* **24**(2019), 667 (2019). <https://doi.org/10.1016/j.prostr.2020.02.059>
90. Zhu, L., Feng, R., Li, X., Xi, J., Wei, X.: A tree-shaped support structure for additive manufacturing generated by using a hybrid of particle swarm optimization and greedy algorithm. *J. Comput. Inf. Sci. Eng.* **19**(4), 1 (2019). <https://doi.org/10.1115/1.4043530>
91. Morgan, D., Agba, E., Hill, C.: Support structure development and initial results for metal powder bed fusion additive manufacturing. *Procedia Manuf.* **10**, 819 (2017). <https://doi.org/10.1016/j.promfg.2017.07.083>
92. Weber, S., Montero, J., Petroll, C., Schäfer, T., Bleckmann, M., Paetzold, K.: The fracture behavior and mechanical properties of a support structure for additive manufacturing of Ti–6Al–4V. *Crystals* (2020). <https://doi.org/10.3390/cryst10050343>
93. Järvinen, J.P., Matilainen, V., Li, X., Piili, H., Salminen, A., Mäkelä, I., Nyrhilä, O.: Characterization of effect of support structures in laser additive manufacturing of stainless steel. *Phys. Procedia* **56**(C), 72 (2014). <https://doi.org/10.1016/j.phpro.2014.08.099>
94. Moller, T., Trumbore, B.: Fast, minimum storage ray-triangle intersection. *Doktorsavhandlingar vid Chalmers Tekniska Hogskola* **2**(1), 109 (1998). <https://doi.org/10.1080/10867651.1997.10487468>
95. Yadroitsev, I., Bertrand, P., Smurov, I.: Parametric analysis of the selective laser melting process. *Appl. Surf. Sci.* **253**(19), 8064 (2007). <https://doi.org/10.1016/j.apsusc.2007.02.088>
96. Aboulkhair, N.T., Maskery, I., Tuck, C., Ashcroft, I., Everitt, N.M.: On the formation of AlSi10Mg single tracks and layers in selective laser melting: microstructure and nano-mechanical properties. *J. Mater. Process. Technol.* **230**, 88 (2016). <https://doi.org/10.1016/j.jmatprotec.2015.11.016>
97. Samantaray, M., Nath Thatoi, D., Sahoo, S.: Finite element simulation of heat transfer in laser additive manufacturing of AlSi10Mg powders. *Mater. Today Proc.* **22**, 3001 (2019). <https://doi.org/10.1016/j.matpr.2020.03.435>
98. Li, Q., Gnanasekaran, B., Fu, Y., Liu, G.R.: Prediction of thermal residual stress and microstructure in direct laser metal deposition via a coupled finite element and multiphase field framework. *JOM* **72**(1), 496 (2020). <https://doi.org/10.1007/s11837-019-03922-w>

99. Song, X., Feih, S., Zhai, W., Sun, C.N., Li, F., Maiti, R., Wei, J., Yang, Y., Oancea, V., Romano Brandt, L., Korsunsky, A.M.: Advances in additive manufacturing process simulation: residual stresses and distortion predictions in complex metallic components. *Mater. Des.* **193**, 108779 (2020). <https://doi.org/10.1016/j.matdes.2020.108779>
100. Mele, M., Bergmann, A., Campana, G., Pilz, T.: Experimental investigation into the effect of supports and overhangs on accuracy and roughness in laser powder bed fusion. *Opt. Laser Technol.* **140**, 1 (2021). <https://doi.org/10.1016/j.optlastec.2021.107024>
101. Whoistylor. Bottle Opener (2015). <https://www.thingiverse.com/thing:655148>

Publisher's Note Springer Nature remains neutral with regard to jurisdictional claims in published maps and institutional affiliations.